Journal of the European Ceramic Society 23 (2003) 505–513

www.elsevier.com/locate/jeurceramsoc

Synthesis of $BaTiO_3$ by applying the sample controlled reaction temperature (SCRT) method to the thermal decomposition of barium titanyl oxalate

F.J. Gotor*, L.A. Pérez-Maqueda, J.M. Criado

Instituto de Ciencia de Materiales de Sevilla, Centro mixto CSIC/Universidad de Sevilla, Centro de Investigaciones Isla de la Cartuja, Avda. Americo Vespucio SN, 41092 Seville, Spain

Received 20 September 2001; received in revised form 20 March 2002; accepted 11 April 2002

Abstract

$BaTiO_3$ samples with a tailored microstructure, specific surface areas ranging from 6.5 to 18.5 m^2/g, were obtained from the thermal decomposition of barium titanyl oxalate (BTO) by using a sample controlled reaction temperature (SCRT) method. These samples are constituted by nanosized crystallites with cubic structure. The use of reducing atmosphere promotes the size diminution of the coherently diffraction domains. The crystallite size and the strain of powdered $BaTiO_3$ samples were measured in several crystallographic directions by using the Warren-Averbach multiple order method. The results have shown that crystallite size is isotropic, whereas the strain has a marked anisotropic character.

Keywords: $BaTiO_3$ and titanates; Calcination; Grain size; SCRT; X-ray methods

1. Introduction

Electronic ceramics—dielectrics, integrated circuit packaged, piezoelectrics, superconductors and magnets—possess the largest share of the advanced ceramic market. Physical properties of these ceramics depend mainly on chemical composition and microstructure, achieved by a careful control of all stages involved during the ceramic processing: powder synthesis, consolidation and forming, sintering, machining, and inspection. The performance of a ceramic component is greatly influenced by powder characteristics such as chemical purity and particle size distribution. Given the overriding need to obtain pure submicronic powders with a tailored size distribution, many researches have focused on the development of low-temperature synthesis methods. However, these novel methods are in general very expensive in comparison with the current powder manufacturing techniques.

Ceramic materials based on ferroelectric $BaTiO_3$ have been dominant in the manufacture of multilayer ceramic capacitors (MLCCs) for the past 45 years. For example, in 1998, the ceramic capacitor industry used ~11,000 tons of $BaTiO_3$-based dielectric materials, which represents nearly 90% of total consumption. Miniaturisation of MLCCs with high capacitance requires the reduction of the dielectric layer thickness accompanied with the increase of the number of active layers. Application of $BaTiO_3$ ceramics has encountered some technical problems such as the strong dependence of capacitance on dc bias, the large temperature coefficient of capacitance, the large grain size, the high dissipation factor and the high sintering temperature. Considerable efforts have been expended in the search for new materials with higher dielectric constant. Lead-based ferroeletric relaxors are promising candidate materials. However, they are difficult to fabricate productively without the formation of a pyrochlore phase that can be detrimental to the dielectric property.[1] The total substitution of $BaTiO_3$ by other dielectric materials in the manufacture of electronic devices is far away to be realised.

Decreasing the dielectric layer thickness in MLCCs preferably down to 2 μm needs small and uniform particle size (100–300 nm). A great number of wet methods for the synthesis of $BaTiO_3$-based materials have been developed over 50 years to attain this goal. These processes are generally classified on the basis of the starting

* Corresponding author.
E-mail address: fgotor@cica.es (F.J. Gotor).

0955-2219/02/$ - see front matter
PII: S0955-2219(02)00099-7

precursors. Among these are acetates, alkoxides, chlorides, hydroxides, nitrates, citrates or oxalates. The first method developed was the thermal decomposition of the barium titanyl oxalate,[2–4] which is very appropriate for obtaining powders with precise stoichiometry and in large quantities. Another coprecipitation method derived from the Pechini synthesis[5] is the citrate process.[6–8] Hydrotermal synthesis,[9,10] sol-gel process[11–13] and hydrolytic decomposition of alkoxides[14,15] are other methods reported in the literature. Chandler et al.[16] have published a review concerning the solution routes to perovskite-phase mixed-metal oxides from metal-organic precursors.

At present, new methods are been still developed specially in order to minimise the temperature at which the crystalline ceramic is observed, with the promise of precise control of microstructure and properties.[17–19] However, the market for chemical synthesised $BaTiO_3$ is surprisingly still very low.[20] Industrial application of these synthesis processes is difficult because of the high cost of precursors, the large shrinkage during processing and the possibility of long processing times. Also, the reproducibility on the quality and physical properties of the final product in mass production is in many cases not enough to ensure the reliability of MLCC manufacturing.

Synthesis researches have mainly focused on the chemistry of the precursor with little attention to the characteristic of the final powder. In general, the required step of the precursor thermolysis consists exclusively of an isothermal calcination in static air. However, the control of experimental parameters involved during the thermal decomposition of the precursor can lead to the improvement of properties of the final product. In this sense, the sample controlled reaction temperature (SCRT) method is especially well adapted to control efficiently the thermal path followed by the sample. Very promising results have been already obtained in the preparation of microporous aluminas from the thermal decomposition of gibbsite[21] or in the synthesis of silicon carbide whiskers from carbothermal reduction of silica gel.[22] More recently, SCRT has been used successfully in the synthesis of hematite and maghemite with tailored porosity from the thermal decomposition of goethite and lepidocrocite, respectively.[23–25] In SCRT, the rate of the transformation (normally a thermal decomposition) is kept constant instead of temperature. In this case, heat and mass transfer phenomena (generated by the rate of the reaction itself) that can affect the reaction kinetics are reduced. The reaction takes place simultaneously within the whole sample and the degree of synchronism is only limited by the sample grain size. This technique permits the control at the same time as the reaction rate and the self-generated partial pressure in the close vicinity of each individual grain. In the field of multilayer capacitors, Dwivedi and Speyer[26] have shown the advantages of this kind of thermal schedule control in the organic burnout of multilayer PZT green ceramics. They have pointed out that a controlled weight loss allows obtaining defect-free specimens.

In this work, ultrafine $BaTiO_3$ powders with a nanometric microstructure have been synthesised from the thermal decomposition of a very common precursor, the barium titanyl oxalate, by means of the SCRT method. SCRT method allows us to tailor the powder microstructure simply by changing the operating conditions, e.g. the rate of the reaction and the self-generated partial pressure.

2. Experimental procedure

2.1. Synthesis of the $BaTiO_3$ powders

$BaTiO_3$ samples were obtained by the thermal decomposition of barium titanyl oxalate, $BaTiO(C_2O_4)_2.4.5H_2O$ (BTO hereafter). The barium titanyl oxalate precursor was prepared as reported by Clabaugh et al.[2] using $BaCl_2.2H_2O$ (Merck, 99%), $TiCl_4$ (Aldrich, 99.995%) and $H_2C_2O_4.2H_2O$ (Merck, 99%) as raw materials. High-resolution X-ray diffraction studies of this precursor[27,28] showed that the Clabaugh synthesis method lead to a single-phase product with a Ba/Ti ratio equal to one. Pure and stoichiometric $BaTiO_3$ powders were obtained from the thermal decomposition of the BTO precursor as checked by X-ray fluorescence analysis.

2.2. SCRT equipments

The thermal decomposition of BTO was carried out under vacuum or gas flow using the sample controlled reaction temperature (SCRT) method. This method aims to control the temperature of the reaction in such a way that the reaction rate is maintained constant all over the process at a value previously selected by the user. A scheme of the SCRT equipment used for controlling the thermal decomposition of BTO under vacuum is shown in Fig. 1. The reactor containing a crucible with the sample was connected to a conventional high vacuum system equipped with pirani and penning gages that allow the measurement of the pressure inside the system in the range from 10^{-6} mbar up to 10 mbar. The analogical output of either the pirani or the penning gage (that is directly proportional to pressure inside the reaction chamber) was connected to the PID controller that monitors the furnace temperature. Thus, the temperature was controlled in such a way that the pressure of the gases generated in the reaction was maintained constant at a value previously selected in the range 10^{-6}–10 mbar. The pumping rate of the vacuum system was also previously selected by means of a butterfly

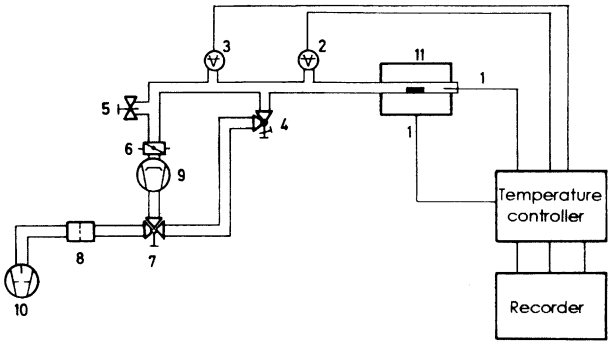

Fig. 1. Sample controlled reaction temperature (SCRT) equipment (1) Thermocouple, (2) penning gage, (3) pirani gage, (4) leak valve, (5) venting valve, (6) butterfly valve, (7) valve, (8) alumina tramp, (9) diffusion pump, (10) rotary pump and (11) furnace.

high vacuum valve. Provided that the gases coming from the thermal decomposition of BTO were pumped at a constant rate and the pressure was maintained constant, the rate at which the gases were produced and, as a consequence, the BTO decomposition rate were necessarily constant all over the process.

A CI electronic microbalance with sample weight capacity up to 5 g was used for the SCRT decomposition of BTO under flow of oxygen or hydrogen. A flow rate of 100 cc/min of hydrogen or oxygen at a total pressure of 1 bar was used. The microbalance is provided with an analogical output proportional to the total change of weight, w, and another one proportional to the rate of change of weight, dw/dt. This arrangement permits the simultaneous measurement of w and dw/dt. The control of the decomposition rate of BTO was achieved by interfacing the dw/dt analogical output to the PID temperature controller.

2.3. X-ray powder diffraction

X-ray powder diffraction diagrams were collected using a D500 Siemens instrument. A strictly monochromatic Cu $K_{\alpha 1}$ radiation ($\lambda = 1.540598$ Å) was produced with an incident beam curved-crystal germanium monochromator with asymmetric focussing. The alignment of the diffractometer was better than 0.005° (2θ). The (111) and (222) reflections of $BaTiO_3$ are the only ones that remain unsplitted on the XRD pattern of the tetragonal phase with regards to the cubic phase. The full-width of the half maximum (FWHM) of (111) diffraction peak was used for calculating the medium diameter of the coherently diffracting domain according to the Scherrer equation. The broadening of the powder patterns due to the particle size and strain contributions was analysed by the Warren-Averbach multiple order method[29,30] from the reflections (100), (110), (111), (200), (220) and (222).

The splitting of the (200) XRD peak of the $BaTiO_3$ cubic phase in the (200) and (002) ones of the tetragonal phase has been very often used for discerning the crystalline structure of $BaTiO_3$. However, the broadening of the XRD peaks in samples with very small crystal sizes would lead to the overlapping of these peaks in the tetragonal samples, what would make very difficult to discern the crystalline structure of $BaTiO_3$ from the analysis of the symmetry of the (200) peak. The Rietveld method has been used here for checking the crystalline structure of $BaTiO_3$ samples in which the splitting of the (200) peak was not apparent. For this purpose, the diffraction pattern was scanned from 20 to 115° (2θ) with a step length of 0.004° and a fixed counting time of 60 s.

2.4. Surface area measurements

Surface area measurements of $BaTiO_3$ samples were carried out with an Adsorpmeter Micromeritic model 2000, using as adsorbate N_2 at the liquid nitrogen temperature.

3. Results and discussion

Table 1 shows the morphological characteristics of the $BaTiO_3$ powders obtained from the SCRT method

Table 1
Specific surface area (S_{BET}), medium particle size (D_{ss}), and size of the coherently diffraction domain (D_{111}) of $BaTiO_3$ samples

Sample	Method	Atmosphere	Pressure (mbar)	Rate (min^{-1})	S_{BET} (m^2/g)	D_{SS} (nm)	D_{111} (nm)
1	SCRT	Vacuum	1×10^{-4}	7.1×10^{-4}	18.3	55	12
2	SCRT	Vacuum	1×10^{-3}	6.8×10^{-4}	15.2	66	12
3	SCRT	Vacuum	2×10^{-2}	3.0×10^{-3}	14.4	69	12
4	SCRT	Vacuum	2×10^{-2}	1.7×10^{-3}	13.2	76	13
5	SCRT	Vacuum	2×10^{-2}	3.9×10^{-4}	14.2	70	13
6	SCRT	Vacuum	2×10^{-2}	2.0×10^{-4}	13.8	72	14
7	SCRT	Vacuum	1×10^{-1}	3.0×10^{-4}	10.6	94	18
8	SCRT	Vacuum	3×10^{1}	7.3×10^{-4}	6.5	154	19
9	SCRT	Oxygen flow	10^3	1.7×10^{-3}	16.0	62	19
10	SCRT	Hydrogen flow	10^3	1.7×10^{-3}	17.0	59	13
11	Isotherm 750 °C	Static air	10^3	–	7	143	33
12	Isotherm 900 °C	Static air	10^3	–	4.5	222	53

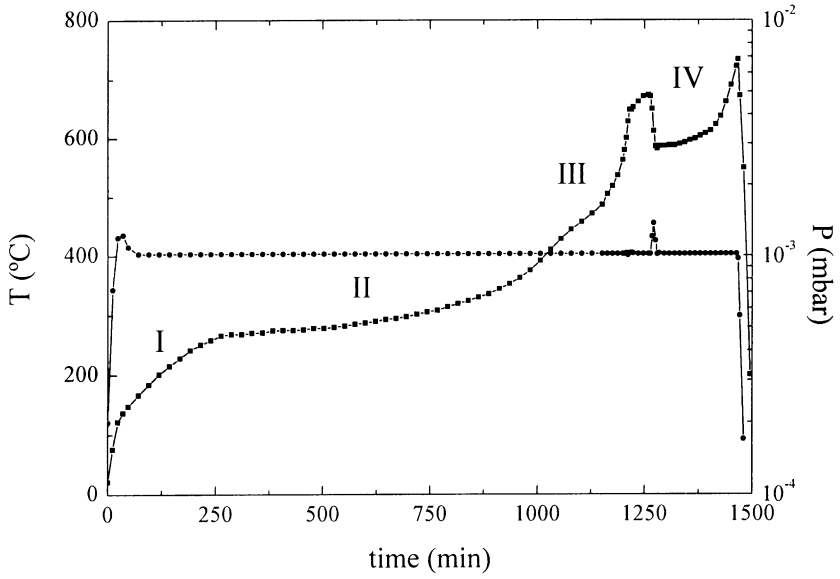

Fig. 2. Temperature (■) and pressure (●) as a function of the time for the thermal decomposition of BTO during a SCRT experiment carried out at a constant pressure of 10^{-3} mbar and a constant rate of 6.8×10^{-4} min^{-1} (sample 2 in Table 1).

under different experimental conditions. This table shows the specific surface area, the medium particle size D_{ss}—calculated from the BET surface by assuming spherical symmetry—and, the size of the coherently diffraction domain D_{111}-calculated from the FWHM of the (111) diffraction peak by the Scherrer method.

Full conversion to $BaTiO_3$ was reached at temperatures as low as 725 °C if the synthesis is carried out under vacuum as illustrated in Fig. 2 (samples 1–8). This figure shows the thermal path followed by sample 2 to ensure a constant partial pressure of 10^{-3} mbar all over the process and, therefore, a constant decomposition rate of 6.8×10^{-4} min^{-1}. Similar SCRT traces were obtained for all the samples described in Table 1. The SCRT diagram of Fig. 2 shows that the thermal decomposition of BTO is a complex process in which four steps seem to be observed. It must be pointed out that these results are similar to those obtained in previous references[28,31] from rising temperature experiments carried out under open-air atmosphere. The successive steps have been attributed to the loss of water molecules from the lattice and to the formation of oxysalts and barium carbonate as by products.[32–34] Thus, it seems to be clear that the difference that would exist between the texture and structure of the $BaTiO_3$ obtained from SCRT experiments and other conventional isotherm or non-isothermal experiments cannot be attributed to differences in the reaction mechanism. The advantage of SCRT is to control the reaction temperature through a precise control of both the partial pressure of the gases generated in the reaction and their own reaction rate, which allows us to minimise the heat and mass transfer phenomena on the whole process.

As observed in Fig. 2, the SCRT process is over when no more gas is released, e.g., when the precursor is completely decomposed and transformed into $BaTiO_3$. But the temperature of the samples was allowed to reach 750 °C and maintained at this temperature for 1 h in order to normalise the final thermal treatment for all the samples. $BaTiO_3$ samples obtained in vacuum from BTO were black due to a carbon residue produced by partial disproportionation of CO. Calcination at 500 °C in flowing oxygen burned out carbon without textural modification of $BaTiO_3$ samples.

SCRT traces corresponding to the decomposition of the BTO precursor under oxygen or hydrogen gas flow are very similar in shape to those obtained under vacuum. However, under gas flow the BTO decomposition occurs at a lower temperature. The normalisation temperature at which all the samples were maintained for 1 h was chosen as 700 °C.

In order to compare the characteristics of the samples obtained by the SCRT method with those obtained from conventional heating methods, the characteristics of two samples prepared by annealing the BTO precursor in static air at 750 and 900 °C for 8 h are also shown in Table 1. Conversion to $BaTiO_3$ in static air from the thermal decomposition of BTO is not completed at least up to 700–800 °C according to previous references.[35–37] The X-ray powder diffraction diagram of the sample annealed in static air at 750 °C (sample 11 in Table 1) still shows the presence of $BaCO_3$ as impurity phase (Fig. 3a). This phase was eliminated when the BTO precursor was calcined at 800 °C. However, Fig. 3b points out that the X-ray powder diffraction pattern of the sample 3 in Table 1 obtained from the SCRT

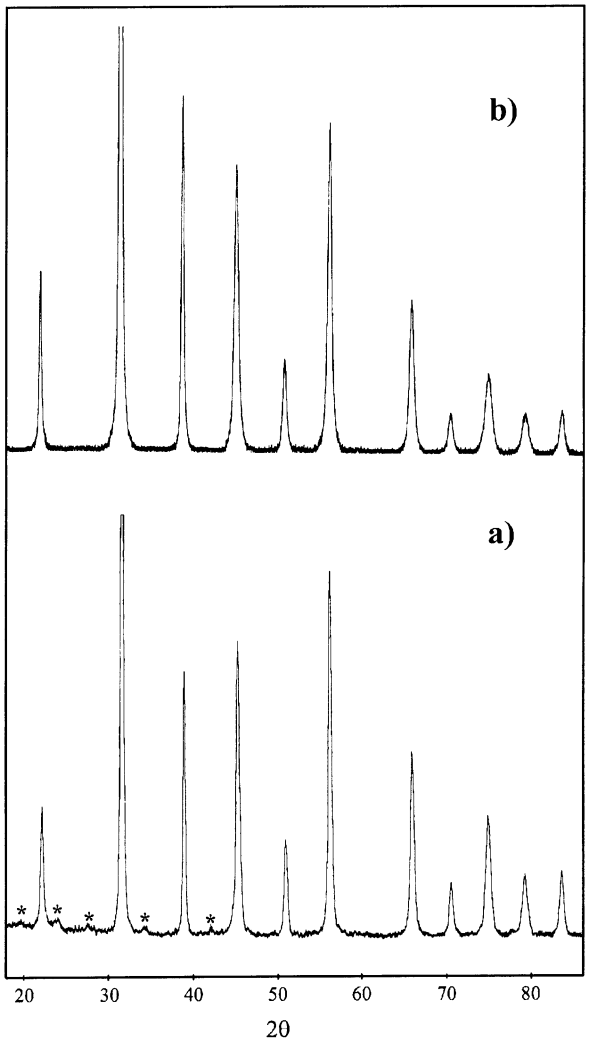

Fig. 3. X-ray powder diffraction patterns: (a) sample 11 and (b) sample 3 (see Table 1) (∗) $BaCO_3$.

method does not evidence the existence of $BaCO_3$, despite the final annealing temperature being 750 °C.

Results in Table 1 show that the microstructure of $BaTiO_3$ samples depends on the experimental conditions used during the calcination of the BTO precursor. For samples obtained from SCRT in vacuum, a relationship between S_{BET} and the set pressure used during the process exists. Higher surface areas are obtained as the pressure of the residual gases maintained constant all over the process is decreased. However, for a given residual pressure, changes in the reaction rate do not affect the final powder microstructure. A similar relationship has been found between the crystallite size and the partial pressure of the gases self-generated on the reaction. Thus, the results included in Table 1 shows that a decrease of D_{111} takes place by decreasing the constant pressure selected in the SCRT experiment. This dependence on the residual pressure would be explained assuming that the reducing conditions used in SCRT experiments generate oxygen deficiencies that can favour the formation of fine-size grains. Oxygen deficiencies must be accompanied by changes in the oxidation state of Ti. Cho et al.[38] have found by XPS Ti^{3+} ions in $BaTiO_3$ samples obtained from a citrate polyester resin precursor. These authors also assumed that the reducing conditions induced by the thermal decomposition of organic substances may produce oxygen vacancies and hence charge compensation in the nearest-neighbour Ti atoms.

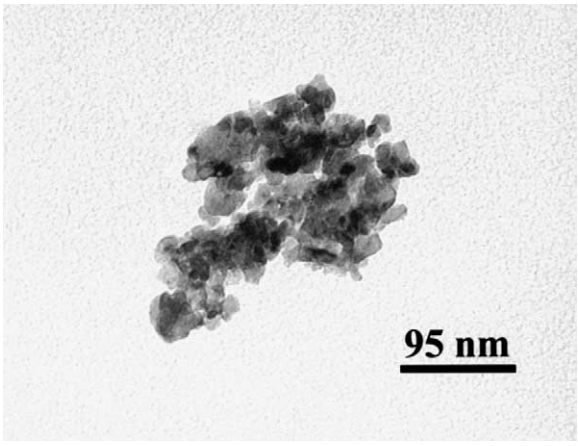

Fig. 4. TEM micrograph of sample 10 in Table 1.

For samples obtained by SCRT under gas flow, an influence of the gas medium on the coherently diffraction domain (D_{111}) was observed. Samples obtained in an oxygen atmosphere have bigger coherently diffraction domains than samples obtained under hydrogen. This result supports the assumption that oxygen vacancies would hinder the growth of $BaTiO_3$ crystallites.

The difference found between the values of the particle size, D_{SS}, calculated from the specific surface area and the corresponding crystal size determined from XRD suggests that $BaTiO_3$ particles are constituted of small crystallites (coherently diffracting domains) welded in a mosaic structure. This is confirmed in Fig. 4, where a TEM image of sample 10 is shown. Similar TEM images were obtained for all the samples synthesised by the SCRT method. Grain size from TEM images agrees with values obtained from XRD, which confirms that $BaTiO_3$ samples have a nanometric microstructure.

Table 1 shows that the SCRT method allows us to obtain $BaTiO_3$ samples with a tailored microstructure by changing the experimental conditions for the BTO calcination. $BaTiO_3$ powders with specific surface area of 18.3 m^2/g was synthesised by this procedure. Data found in the literature about the specific surface area or grain size of $BaTiO_3$ powders obtained from the thermal decomposition of BTO are generally similar to results obtained by us for sample 11. Until our results, only Saegusa et al.[39] have reported $BaTiO_3$ powders with higher S_{BET}, 20 m^2/g, than these reported by using the thermal decomposition of BTO. In this case, the authors

modified the Clabaugh method for the BTO synthesis in order to reduce the microstructure and/or the final temperature of calcination of the precursor. They have shown that the morphology of the precursor particles is maintained in the $BaTiO_3$ powder obtained as the final product.[39] At this point, it must been remembered that the BTO precursor used in our work was synthesised of the original Clabaugh method and it was constituted by small single crystals.

Similar powder microstructure has been obtained from more sophisticated wet chemical methods. For instance, $BaTiO_3$ powders obtained by the citrate or alkoxide route show a surface area of ~15 or 21 m^2/g, respectively.[7] A controlled double-jet precipitation technique (CDJP) produces powders with 12 or 25 m^2/g of surface area depending on the method of introducing the $BaCl_2$ and $TiCl_4$ reactant solutions into the reactor.[37] The highest surface areas were obtained from low-temperature aqueous synthesis. Nanni et al.[40] have prepared $BaTiO_3$ powders with S_{BET} higher than 39 m^2/g.

It was proposed in previous references[41,42] that the stabilization of the cubic phase with regards to the tetragonal one depends on the size of the coherently diffraction domains (crystallite size) rather than on the particle size as concluded by Uchino et al.[43] It was suggested[41,42] that the cubic phase of $BaTiO_3$ is stabilised for crystallite sizes smaller than 15 nm. The analysis of the symmetry of the (002) and (200) does not seem to be an accurate method for discerning if the sample is either tetragonal or cubic. Sharma and Mc Carthey[44] have suggested that the broadening of the XRD profiles because of the small particle size would raise from the splitting of (002) and (200) reflections leading to a symmetric appearance that would lead to the erroneous conclusion that a tetragonal $BaTiO_3$ sample has a cubic symmetry. However, it is necessary to point out that contradictory opinion can be found in the recent literature[43–47] regarding the analysis of the splitting of the (002) and (200) peaks for discerning between cubic and tetragonal symmetry. Thus, the fitting of the XRD data by the Rietveld method, instead of the symmetry analysis of the (002) and (200) peaks, has been used for checking the structure of samples. Both the integrated intensities and the peak positions of the XRD diagrams recorded for the set of samples included in Table 1 have been fitted by means of the Rietveld refinement program FULLPROF.[48] Fig. 5 shows by way of example the XRD diagram of the sample labelled 3 in Table 1 recorded from 20° (2θ) up to 145° (2θ) and the difference between the observed and calculated pattern. The conditions of the refinement are included in Table 2. The excellent fitting parameters shown in this table demonstrate that this $BaTiO_3$ sample presents cubic structure. Similar good fittings have been obtained for the set of samples reported in Table 1 that have been synthesised using the SCRT method. It is noteworthy to point out

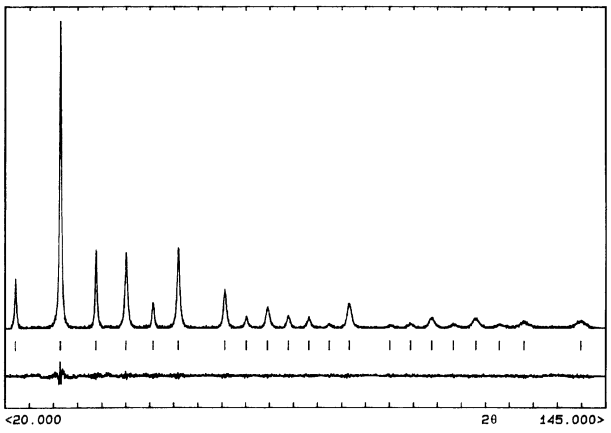

Fig. 5. Final Rietveld plot for sample 3: the observed data, the positions calculated for Bragg reflections and the difference between observed and calculated patterns.

that it has not been possible to fit by the Rietveld method by assuming a cubic symmetry the XRD profiles of those samples that have been obtained by conventional heating under open atmosphere (labelled 11 and 12 in Table 1). These results support the conclusion that the cubic phase of $BaTiO_3$ is stabilised with regard to the tetragonal phase when the averaged crystallite size is smaller than about 15 nm.

The analysis of both the average crystallite size and the level of microstrains in different crystallographic directions by means of a Fourier analysis would allow a better knowledge of the microstructural characteristics of barium titanate with nanosized coherently diffraction domains. This study can be carried out for cubic $BaTiO_3$ samples because in such a case the splitting of the diffraction peaks characteristic of the tetragonal structure does not take place. The crystallite size and the main square strains were analysed by way of example for the samples 3 and 8 of the Table 1 by considering three different crystallographic directions using the three following pairs of XRD reflections: (100, 200), (110, 220) and (111, 222). The plots of the domain-size coefficient, A_L^S, and the mean square strain, $<\varepsilon^2>^{1/2}$,

Table 2
Details of the Rietveld refinement for sample 3 in Table 1

a (Å)	4.018 (2)
V (Å^3)	64.9 (3)
Z	1
Space group	Pm 1 3 m
2θ range (°)	20–145
Step size (°)	0.04
No. of reflections	21
R_p	0.0032
R_{wp}	0.042
R_F	0.032
R_B	0.048

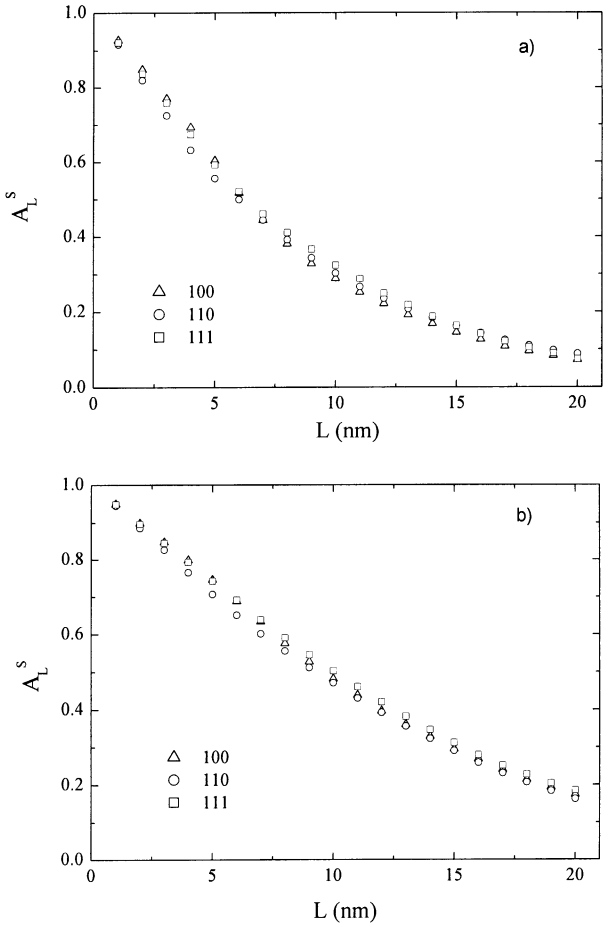

Fig. 6. Fourier size coefficients A_L^S vs L for [100], [110] and [111] directions: (a) sample 3 and (b) sample 8 (see Table 1).

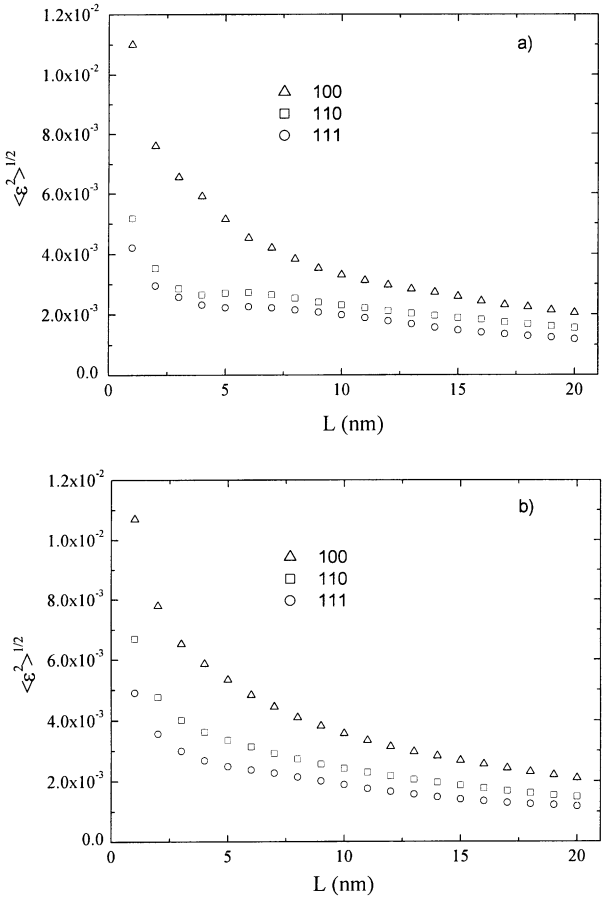

Fig. 7. The mean square strain $<\varepsilon^2>^{1/2}$ vs L in the [100], [110] and [111] directions: (a) sample 3 and (b) sample 8 (see Table 1).

Table 3
Calculated Fourier apparent sizes for samples 3 and 8 in Table 1

Sample	hkl	ε_F (nm)
3	100	13
	110	11
	111	12
8	100	20
	110	17
	111	19

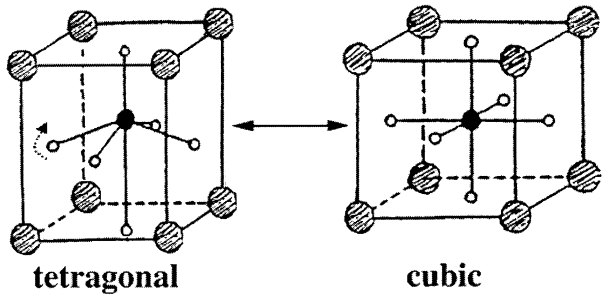

Fig. 8. Rearrangement of the oxygen atoms during the tetragonal/cubic transformation of $BaTiO_3$.

versus the real distance perpendicular to the reflecting plane, L, are included in Figs. 6 and 7, respectively. Fig. 6 shows that the A_L^S versus L plots of the different crystallographic directions are overlapping, which means that the average crystallite size has an isotropic behaviour and the crystallites are spherically shaped. Apparent crystallite size, ε_F, has been estimated by extrapolating the linear part of the plots in Fig. 6, which intercept the L axis at $L=\varepsilon_F$. The results summarised in Table 3 confirm the isotropic distribution of the crystallite size in all the directions.

On the other hand, the analysis of the results included in Fig. 7 points out that the distribution of microstrains in the nanosized $BaTiO_3$ is anisotropic. It can be observed that the level of strains in the direction [100] is considerably higher than those across the [110] and [111] directions. This behaviour would be explained by considering that, as shown in Fig. 8, the stabilisation of the cubic phase at room temperature implies a displacement of the oxygen atoms of the tetragonal phase in the direction perpendicular to the (100) planes, which would generate a high level of microstrains in these planes.

4. Conclusions

The use of the SCRT method for obtaining $BaTiO_3$ from the thermal decomposition of barium titanyl oxalate has been shown to have several advantages over conventional isothermal treatments. This method allows an accurate control of the experimental conditions that permits the considerable reduction of the calcination temperature and to improve the quality of the final product by tailoring its microstructure. $BaTiO_3$ powders with specific surface area higher than 18 m^2/g have been synthesised using this procedure. The as prepared samples were constituted by nanosized crystallites with cubic structure. The study of the broadening of XRD patterns of the $BaTiO_3$ samples by means of the Warren–Averbach method has shown that the crystal size is independent of the crystalline direction (i.e., they have a spherical shape) while the level in microstrains is clearly higher in the [100] direction. This behaviour has been explained by considering that the tetragonal → cubic transformation of $BaTiO_3$ is accomplished through a rearrangement of the oxygen atoms that implies a slight displacement in the perpendicular direction to (100) planes.

References

1. Shrout, T. R. and Hallival, A., Preparation of lead-based ferroelectric relaxors for capacitorts. *Am. Ceram. Soc. Bull.*, 1987, **66**, 704–711.
2. Clabaugh, W. S., Swiggard, E. M. and Gilchrist, R., Preparation of barium titanyl oxalate tetrahydrate for conversion to barium titanate of high purity. *J. Res. Natl. Bur. Std*, 1956, **56**, 289–291.
3. Fang, T. T. and Lin, H. B., Factors affecting the preparation of barium titanyl oxalate tetrahydrate. *J. Am. Ceram. Soc.*, 1986, **72**, 1899–1906.
4. Hsiang, H. I. and Yen, F. S., Effect of crystallite size on the ferroelectric domain growth of ultrafine $BaTiO_3$ powders. *J. Am. Ceram. Soc.*, 1996, **79**, 1053–1060.
5. Pechini, M. P., Method of preparing lead and alkaline earth titanates and niobates and coatings using the same to form a capacitor. US Patent 3 330 697, 11 July, 1967.
6. Hutchins, G. A., Maher, G. H. and Ross, S. D., Control of the Ba:Ti ratio of $BaTiO_3$ at a value of exactly 1 via conversion to BaO $TiO_2 3C_6H_8O_7$. $3H_2O$. *Am. Ceram. Soc. Bull.*, 1987, **66**, 681–684.
7. Rajendran, M. and Suba Rao, M., Formation of $BaTiO_3$ from citrate precursor. *J. Solid State Chem.*, 1994, **113**, 239–247.
8. Tsay, J. D. and Fang, T. T., Effects of temperature and atmosphere on the formation mechanism of barium titanate using the citrate process. *J. Am. Ceram. Soc.*, 1996, **79**, 1693–1696.
9. Vivekanandan, R., Philip, S. and Kutty, T. R. N., Hydrothermal preparation of $Ba(Ti,Zr)O_3$ fine powders. *Mater. Res. Bull*, 1986, **22**, 99–108.
10. Xia, C. T., Shi, E. W., Zhong, W. Z. and Guo, J. K., Preparation of $BaTiO_3$ by the hydrothermal method. *J. Eur. Ceram. Soc.*, 1995, **15**, 1171–1176.
11. Clark, I. J., Takeuchi, T., Ohtori, N. and Sinclair, D. C., Hydrothermal synthesis and characterisation of $BaTiO_3$ fine powders: precursors, polymorphism and properties. *J. Mater. Chem.*, 1999, **9**, 83–91.
12. Yoko, Y., Kamiya, K. and Tanaka, K., Preparation of multiple oxide $BaTiO_3$fibres by the sol-gel method. *J. Mater. Sci.*, 1990, **25**, 3922–3929.
13. Viswanath, R. N. and Ramasamy, S., Preparation and ferroelectric phase transition studies of nanocrystalline BaTiO3. *Nanostruct. Mater.*, 1997, **8**, 155–162.
14. Mazdiyasni, K. S., Dollof, R. T. and Smith, J. S. II, Preparation of high-purity submicron barium titanate. *J. Am. Ceram. Soc.*, 1969, **52**, 523–526.
15. Campion, J. F., Payne, D. A., Chae, H. K., Maurin, J. K. and Wilson, S. R., Synthesis of bimetallic barium titanate alkoxides as precursors for electrical ceramics. Molecular structure of the new barium titanium oxide alkoxide $Ba_4Ti_{13}(\mu_3\text{-}O)_{12}(\mu_5\text{-}O)_6(\mu_1\text{-}\eta^1\text{-}OCH_2CH_2OCH_3)_{12}(\mu_1,\mu_3\text{-}\eta^2\text{-}OCH_2CH_2OCH_3)_{12}$. *Inorg. Chem.*, 1991, **30**, 3244–3245.
16. Chandler, C. D., Roger, C. and Hampden-Smith, M. J., Chemical aspects of solution routes to perovskite-phase mixed metal oxides from metal-organic precursors. *Chem. Rev.*, 1993, **93**, 1205–1241.
17. Yoshimura, M., Importance of soft solution processing for advanced inorganic materials. *J. Mater. Res.*, 1998, **13**, 796–802.
18. Beck, Ch, Härtl, W. and Hempelmann, R., Size-controlled synthesis of nanocrystalline $BaTiO_3$ by a sol-gel type hydrolysis in microemulsion-provided nanoreactors. *J. Mater. Res.*, 1998, **13**, 3174–3180.
19. Bocquet, J. F., Chhor, K. and Pommier, C., Barium titanate powders synthesis from solvothermal reaction and supercritical treatment. *Mater. Chem. Phys.*, 1999, **57**, 273–280.
20. Geiger, G., Powder synthesis and shape forming of advanced ceramics. *Am. Ceram. Soc. Bull.*, 1995, **74**, 62–65.
21. Rouquerol, J. and Ganteaume, D., Thermolysis under vacuum: Essential influence of the residual pressure on thermoanalytical curves and the reaction products. *J. Therm. Anal*, 1977, **11**, 201–210.
22. Real, C., Alcala, M. D. and Criado, J. M., Synthesis of silicon carbide whiskers from carbothermal reduction of silica gel by means of the constant rate thermal analysis (CRTA) method. *Solid State Ionics*, 1997, **95**, 29–32.
23. Chopra, G. S., Real, C., Alcalá, M. D., Pérez-Maqueda, L. A., Subrt, J. and Criado, J. M., Factors influencing the texture and stability of maghemite obtained from the thermal decomposition of lepidocrocite. *Chem. Mater.*, 1999, **11**, 1128–1137.
24. Pérez-Maqueda, L. A., Subrt, J., Criado, J. M. and Real, C., Synthesis of acicular hematite catalysts with tailored porosity. *Catal. Letters*, 1999, **60**, 151–156.
25. Pérez-Maqueda, L. A., Criado, J. M., Real, C., Subrt, J. and Bohácek, J., The use of constant rate thermal analysis (CRTA) for controlling the texture of hematite obtained from the thermal decomposition of goethite. *J. Mater. Chem.*, 1999, **9**, 1839–1845.
26. Dwivedi, A. and Speyer, R. F., Rate-controlled burnout of multilayer green ceramics. *Thermochim. Acta*, 1994, **247**, 431–438.
27. Louër, D., Boultif, A., Gotor, F. J. and Criado, J. M., X-ray powder diffraction analysis of barium titanyl oxalate tetrahydrate. *Powder Diffraction*, 1990, **5**, 162–164.
28. Louër, M., Louër, D., Gotor, F. J. and Criado, J. M., Crystal structure of barium titanyl oxalate $BaTiO(C_2O_4)_2 4.5H_2O$. *J. Solid State Chem.*, 1991, **92**, 565–572.
29. Warren, B. E., *X-Ray Diffraction*. Addison-Wesley, Reading, MA, 1969.
30. Louër, D., Weigel, D. and Louboutin, R., Direct method for correcting X-ray diffraction line profiles I. Deconvolution method. *Acta Crystallogr.*, 1969, **A25**, 335–338.
31. Pfaff, G., Schmidt, F., Ludwig, W. and Feltz, A., $M^{II}TiO(C_2O_4)_2 4H_2O$ (M^{II} = Mg, Ca, Sr or Ba) as precursors in the formation of $M^{II}TiO_3$ powders. *J. Therm. Anal*, 1988, **33**, 771–779.

32. Fang, T. T., Lin, H. B. and Hwang, J. B., Thermal analysis of precursors of barium titanate prepared by coprecipitation. *J. Am. Ceram. Soc*., 1990, **73**, 3363–3367.
33. Stockenhuber, M., Mayer, H. and Lercher, J. A., Preparation of barium titanates from oxalates. *J. Am. Ceram. Soc*., 1993, **76**, 1185–1190.
34. Otta, S. and Bhattamisra, S. D., Kinetics and mechanism of the thermal decomposition of barium titanyl oxalate. *J. Therm. Anal*., 1994, **41**, 419–433.
35. Dutta, P. K., Gallagher, P. K. and Twu, J., Raman spectroscopic study of the formation of barium titanate from an oxalate precursor. *Chem. Matter*, 1993, **5**, 1739–1743.
36. Potdar, H. S., Deshpande, S. B. and Date, S. K., Alternative route for synthesis of barium titanyl oxalate: Molecular precursor for microcrystalline barium titanate powders. *J. Am. Ceram. Soc*., 1996, **79**, 2795–2797.
37. Her, Y.-S., Matijevic, E. and Chon, M. C., Preparation of well-defined colloidal barium titanate crystals by the controlled double-jet precipitation. *J. Mater. Res*., 1995, **10**, 3106–3114.
38. Cho, W. S., Hamada, E. and Takayanagi, K., Stacking faults in $BaTiO_3$ particles synthesized from organic precursor. *J. Appl. Phys*., 1997, **81**, 3000–3002.
39. Saegusa, K., Rhine, W. E. and Bowen, H. K., Preparation of stoichiometric fine lead barium titanate powder. *J. Am. Ceram. Soc*., 1993, **76**, 1495–1504.
40. Nanni, P., Leoni, M., Buscaglia, V. and Aliprandi, G., Low-temperature aqueous preparation of barium metatitanate powders. *J. Eur. Ceram. Soc*., 1994, **14**, 85–90.
41. Criado, J. M., Dianez, M. J., Gotor, F., Real, C., Mundi, M., Ramos, S. and del Cerro, J., Correlation between synthesis conditions, coherently diffracting domain size and cubic phase stabilization in barium titanate. *Ferroelectrics Lett*., 1992, **14**, 79–84.
42. Gotor, F. J., Real, C., Dianez, M. J. and Criado, J. M., Relationships between the texture and structure of $BaTiO_3$ and its tetragonal/cubic transition enthalpy. *J. Solid State Chem*., 1996, **123**, 301–305.
43. Uchino, K., Sadanaga, E. and Hirose, T., Dependence of the crystal structure on particle size in barium titanate. *J. Am. Ceram. Soc*., 1989, **72**, 1555–1558.
44. Sharma, N. C. and McCartney, E. R., The dielectric properties of pure barium titanate as a function of grain size. *J. Aust. Ceram. Soc*., 1974, **10**, 16–20.
45. Begg, B. D., Vance, E. R. and Nowotny, J., Effect of particle size on the room-temperature crystal structure of barium titanate. *J. Am. Ceram. Soc*., 1994, **77**, 3186–3192.
46. Arima, M., Kakihana, M., Nakamura, Y., Yashima, M. and Yoshimura, M., Polymerized complex route to barium titanate powders using barium-titanate mixed-metal citric acid complex. *J. Am. Ceram. Soc*., 1996, **79**, 2847–2856.
47. Eckert, J. O. Jr., Hung-Houston, C. C., Gersten, B. L., Lencka, M. M. and Riman, R. E., Kinetics and mechanisms of hydrothermal synthesis of barium titanate. *J. Am. Ceram. Soc*., 1996, **79**, 2929–2939.
48. Rodiguez-Carvajal, J., In: *Collected abstracts of the powder diffraction meeting*. Toulouse, France, 1990 p. 127.